PCCP

COMMUNICATION

View Article Online
View Journal | View Issue

Cite this: *Phys. Chem. Chem. Phys.*, 2025, **27**, 3552

Received 7th November 2024,
Accepted 29th January 2025

DOI: 10.1039/d4cp04258a

rsc.li/pccp

Unusual phase transition mechanism induced by shear strain in Si_2BN planar structures and comparison with graphene: an *ab initio* DFT study

Zacharias G. Fthenakis *[ab] and Madhu Menon *[cd]

Using *ab initio* methods we show that by applying shear strain, a phase transition occurs between the AB and the AA Si_2BN planar sheets. Si–Si bonds stretch and bend towards the strain direction, causing an internal displacement of the remaining almost unchanged Si_2BN strips. As the shear strain increases, Si–Si bonds weaken and break, while leading to new Si–Si bond formation and causing the phase transition. The planar structure is maintained throughout the application of the strain, with no buckling, a phenomenon not reported so far in other 2D materials. Performing the same calculations for graphene we show that its structural deformations are strikingly different and result in buckling.

Recently, it was found that Si_2BN is a stable periodic two-dimensional (2D) structure, which; (i) although containing Si, is entirely planar, (ii) it has a honeycomb structure, very similar to graphene and (iii) it can be stable at temperatures of the order of 1000 K.[1] The structure is composed of alternating Si–Si and B–N bonds along the armchair chains, as shown in Fig. 1(a). Depending on the alternating orientation of the B–N bonds several stable allotropes of the Si_2BN structure may be considered. One of them is shown in Fig. 1(b), which is also planar, and was found to be slightly more stable than the one of Fig. 1(a) (see ref. 2). The two structures of Fig. 1(a) and (b) are the simplest Si_2BN allotropes, which are planar and their combination may produce several other mixed Si_2BN allotropes. In the former, the orientation of B–N bonds along an armchair chain is alternated (B–N and N–B) and the structure can be considered as having an AB stacking. On the other hand, in the latter, the orientation of the B–N bonds along an armchair chain is the same and the structure can be considered as having an AA stacking. More details for the crystalographic structure of those allotropes can be found in ref. 3 where their structural optimizations were performed using the density functional theory (DFT) in the generalized gradient approximation (GGA) with the Perdue–Burke–Ernzerhof (PBE) functional[4] using the SIESTA code.[5] Although Si_2BN has not been synthesized yet, it has been extensively studied for several of its properties, including its electronic,[3] optical,[6] thermoelectric[7] and mechanical properties.[8] It has been shown to be a promising candidate for hydrogen storage,[9–12] as anode materials for Mg-ion batteries,[13,14] as material for gas sensing applications,[15,16] as catalyst,[17] for its interactions with DNA/RNA bases for biosensing applications[18] *etc.* These studies attest to the increasing interest of the scientific community in the properties of the Si_2BN structure.

In the present study we use DFT calculations to show that by applying in-plane shear strain either on the AA or the AB allotrope, the one allotrope can be transformed into the other. This is an unusual phase transition mechanism, belonging to a class of diffusionless (also called displacive) phase transitions, where due to shear strain, the atoms of the parent crystal structure are shifted in an organized manner, creating a new crystalline phase, without any atomic diffusion. These are the main characteristics of a Martensitic phase transition, which appears in many cases of three-dimensional materials, but it is

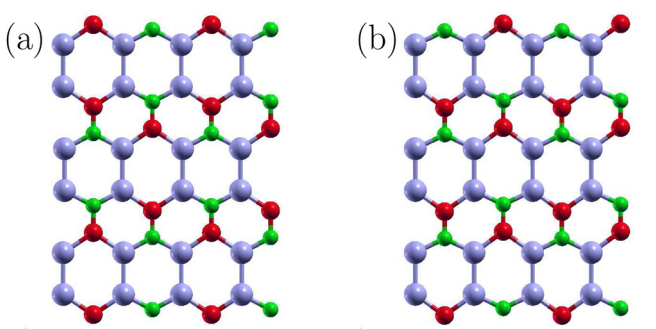

Fig. 1 Si_2BN structures with (a) AB and (b) AA stacking. Blue, red, and green spheres represent Si, B, and N atoms, respectively.

[a] *Istituto Nanoscienze, Consiglio Nazionale delle Ricerche (CNR), 56127 Pisa, Italy. E-mail: zacharias.fthenakis@nano.cnr.it, fthenak@eie.gr*
[b] *National Enterprise for nanoScience and nanoTechnology (NEST), Scuola Normale Superiore, 56127 Pisa, Italy*
[c] *Conn Center for Renewable Energy Research, University of Louisville, Louisville, KY 40292, USA. E-mail: super250@g.uky.edu*
[d] *Department of Physics and Astronomy, University of Kentucky, Lexington, KY 40506, USA*

rarely observed in 2D ones. For instance, the Martensitic phase transition in 2D materials has been reported in the transformation between black and blue phosphorene,[19] the β-GeSe and α-SnTe monolayer multiferroics[20] and the SnSe monochalcogenide.[21] In the case of Si_2BN, that phase transition can be achieved by overcoming a relatively small energy barrier, which is also studied, and shown to be due to the stretching and bending of the relatively weak Si–Si bonds. Under shear strain, each Si–Si bond is bent and eventually broken with a subsequent formation of another Si–Si bond, thus turning the AA structure into AB and *vice versa*. The corresponding mechanism for graphene is also studied for comparison, but no such behavior is observed. Instead, graphene under shear strain is found to buckle out of plane. This can be explained due to the equivalent strength of graphene bonds, which do not allow some of them to bend, without the bending of the others. This also explains that the observed phenomenon of phase change in Si_2BN may occur only in systems with bonds with inequivalent strengths. Therefore, this is not expected to be observed in binary 2D systems like the hexagonal BN, but it might be observed in other ternary 2D systems.

Usually, in the Martensitic phase transitions the atomic displacements are smaller than the spacing between adjacent atoms, and their relative arrangement topologically is preserved. This, however, is not the case for the presented transformation of Si_2BN, since the topology between the two phases is distinctly different in terms of the kind of atoms participating in each hexagonal ring containing the Si–Si bonds. Moreover, upon further application of the shear strain, the phase change will continue to alternate between the two phases. This phase transition mechanism has not been reported for any other 2D material.

For the DFT calculations, we use the SIESTA code[5] in the PBE level[4] and the same parameters as those described in ref. 8 In brief, we utilize (i) norm-conserving Troullier–Martins pseudopotentials[22] in the Kleinman–Bylander factorized form,[23] (ii) an atomic-like double-zeta basis with polarization orbitals for the wave function expansion in real space, (iii) a 10 × 10 × 1 Monkhorst–Pack[24] k-point grid, (iv) a 500 and 300 Ry mesh cutoff energy for Si_2BN and graphene, respectively, for the determination of charge densities and potentials. Starting from the optimized 32-atom rectangular unit cells of Si_2BN and graphene, which are reported in ref. 8 we gradually introduce in-plane shear strain, by modifying the tilting angle ϕ between the lattice vectors **a** and **b**, allowing the length of **a** and **b** to vary. In the unstrained structure, $\mathbf{a} = (a_0, 0, 0)$ and $\mathbf{b} = (0, b_0, 0)$, while in the strained ones, $\mathbf{a} = (a, 0, 0)$ and $\mathbf{b} = b(\sin\phi, \cos\phi, 0)$, with $\varepsilon_{xy} = \tan\phi$ being the shear strain. The vectors **a** and **b**, and the tilt angle ϕ are shown schematically in Fig. 2(a). Moreover, a 20 Å of vacuum is considered in the z direction, to simulate an isolated sheet of the structure. Optimizations are performed for increasing ϕ values with 1° increment and fixed lattice vector lengths using the conjugate gradient method. For each fixed ϕ value the structure is fully optimized both for the atomic positions and the lattice vector lengths. The structure is considered fully optimized if the maximum atomic force becomes smaller than 0.005 eV $Å^{-1}$, and both the in plane stress components σ_{xx} and σ_{yy} become smaller than 0.01 GPa, assuming that the thickness of the Si_2BN and graphene sheet is 3.34 Å (see ref. 25), which is the sheets' separation in graphene.

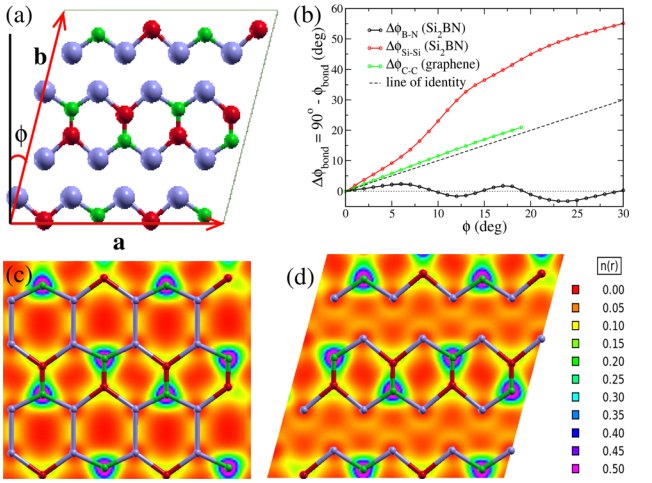

Fig. 2 (a) Lattice vectors **a** and **b**, and the tilt angle ϕ due to shear strain. (b) The evolution with tilt angle ϕ of the angles formed between B–N and Si–Si bonds with **a** in Si_2BN and the angle between the C–C bonds of graphene with **a**, which for $\varepsilon_{xy} = 0$ are normal to **a**. (c) and (d) Electron density for the unstrained AA Si_2BN and for the AB Si_2BN structure under shear strain for $\phi = 15°$, respectively.

In Fig. 3 we show the optimized structures under shear strain of Si_2BN for $\phi = 0, 3°, 6°, 9°\ldots$. Below each snapshot, the tilting angle ϕ and the corresponding shear strain $\varepsilon_{xy} = \tan\phi$ are shown. As one can see, shear strain causes a relatively large tilt in the Si–Si bonds, while the direction of B–N bonds remains almost intact. This can be seen in Fig. 2(b), which shows the angle $\Delta\phi_{bond} = 90° - \phi_{bond}$ as a function of ϕ, where ϕ_{bond} is the angle between the bond direction (B–N or Si–Si) and the lattice vector **a**. Indeed, $\Delta\phi_{B-N}$ is very close to 0, while $\Delta\phi_{Si-Si}$ increases with ϕ, taking values well above ϕ. This figure allows us to consider that Si_2BN consists of strips of hexagons containing the B–N bonds, which are interconnected through the Si–Si bonds and they slide with each other under shear strain. The bond lengths between the atoms of those stripes (*i.e.* the Si–B, Si–N, and B–N bond lengths) are shown in Fig. 4, where one can see that those bonds are deformed only slightly. It is worth noting that two different bonds appear between B and Si and between N and Si, which are shown in Fig. 4 as Si–N(1) and Si–N(2), and Si–B(1) and Si–B(2), respectively. From the bond length values of that figure, one can find that during the transformation from one phase to the other, the Si–N, Si–B, and B–N bonds are not shrunk by more than 3.6% and are not elongated by more than 3.0%.

As shear strain increases, the Si–Si bond tilts are accompanied by a Si–Si bond length increase, causing bond weakening and finally bond breaking. However, before bond breaking, each Si atom of the upper strip comes closer to the next Si atom of the lower strip forming a new Si–Si bond. This can be seen in Fig. 2(c) and (d), which show the electron density for the unstrained AA Si_2BN structure and the AB Si_2BN under shear

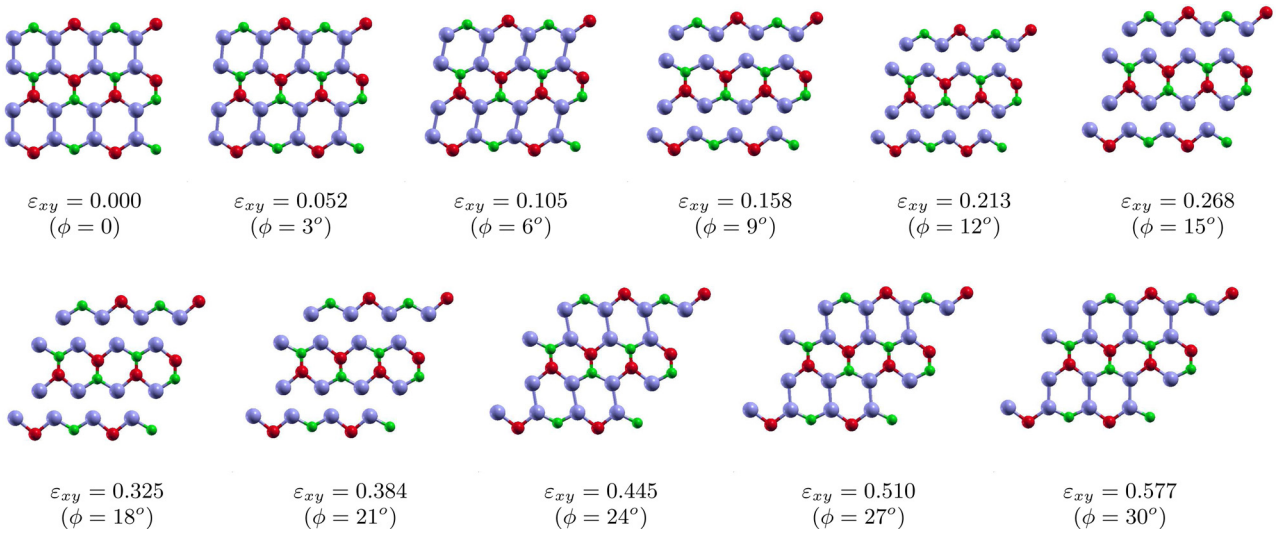

Fig. 3 Transformation of Si_2BN structure with AB stacking into Si_2BN structure with AA stacking by applying shear strain. The snapshots represent the evolution of the optimized structure of AB Si_2BN as shear strain increases. Below each snapshot the shear strain ε_{xy} and the tilting angle between the lattice vectors **a** and **b** are shown. Blue, red, and green spheres represent Si, B, and N atoms, respectively.

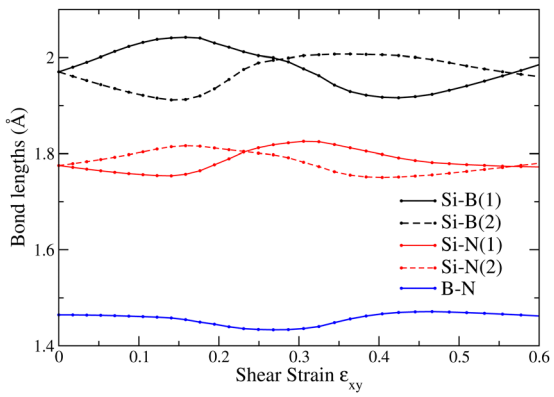

Fig. 4 Si–B, Si–N and B–N bond lengths *versus* shear strain ε_{xy}.

strain for $\phi = 15^\circ$, respectively. In the former, the electrons tend to be in the middle of the Si–Si bond, indicating covalent bonding, which however, due to the small charge density in the area between the Si atoms, is not a very strong bond. In the latter, the electron density has a small valley between the Si atoms, indicating that the electrons prefer to be closer to the Si atoms rather than in the center of the bond and the Si–Si bond starts breaking. At the same time, however, a new Si–Si bond of similar strength has started to form between the Si atom of one strip with the next Si atom of the other strip. Thus, as the shear strain increases, the former Si–Si bond breaks while the new one strengthens, replacing the former, and transforms the AB Si_2BN structure into the AA one and *vice versa*. This bond weakening is shown in Fig. 3 as an absence of Si–Si bond sticks.

On the other hand, the corresponding snapshots for graphene, which are shown in Fig. 5, reveal a totally different behavior. In graphene, the strong C–C bonds allow only a small and uniform bond tilting which is not that large enough to cause any bond breaking. In particular, the corresponding angle $\Delta\phi_{C-C}$ for graphene, which is also shown in Fig. 2(b), almost follows the line of identity $\Delta\phi_{C-C} = \delta\phi$, indicating that the bending of the C–C bonds follows the tilt angle. As ε_{xy} increases, the C–C bond lengths do not change significantly and the calculations show that the planar structure may be retained up to $\varepsilon_{xy} = 0.36$ (or $\phi = 20^\circ$) (see Fig. 5(a)). For larger ε_{xy} values the structure buckles to accommodate the strain, and for $\varepsilon_{xy} = 0.466$ (or $\phi = 25^\circ$), buckling brings closer some C atoms, (which in the unstrained structure would be far apart), which now form bonds and transform the structure into a totally new one with mixed sp^1/sp^2 bonding. This structure is shown in Fig. 5(c). Buckling however, may occur for even smaller ε_{xy} values and our results show that it may start at $\varepsilon_{xy} \approx 0.16$ (or $\phi \approx 10^\circ$). This result was obtained by optimizing the buckled graphene structure found for $\phi = 20^\circ$, for gradually decreasing ϕ values. According to our findings, the energy of the buckled structures is smaller than that of the planar ones for the same ε_{xy} values, and buckling disappears when ϕ drops down to $\phi = 9^\circ$. Snapshots of those buckled graphene structures are shown in Fig. 5(b).

Fig. 6(a) shows the strain energy $\Delta E = E - E_{0,AB}$ per formula unit for the Si_2BN structure with respect to the energy $E_{0,AB}$ of the unstrained Si_2BN structure with AB stacking, while Fig. 6(d) shows the corresponding one for graphene. Fig. 6(d) shows also the energy curve of Si_2BN for comparison. As one can see in Fig. 6(a) the energy barrier for the transformation of Si_2BN with AB stacking into the Si_2BN structure with AA stacking is 0.54 eV per formula unit and corresponds to the value $\varepsilon_{xy} = 0.22$. This relatively small energy barrier indicates that this transformation is achievable. Considering that this process is reversible and the fact that the energy of the optimum Si_2BN structure with AA stacking is smaller than Si_2BN structure with AB stacking by 0.16 eV, the energy barrier for the conversion of AA into AB Si_2BN is 0.70 eV per formula unit. On the other

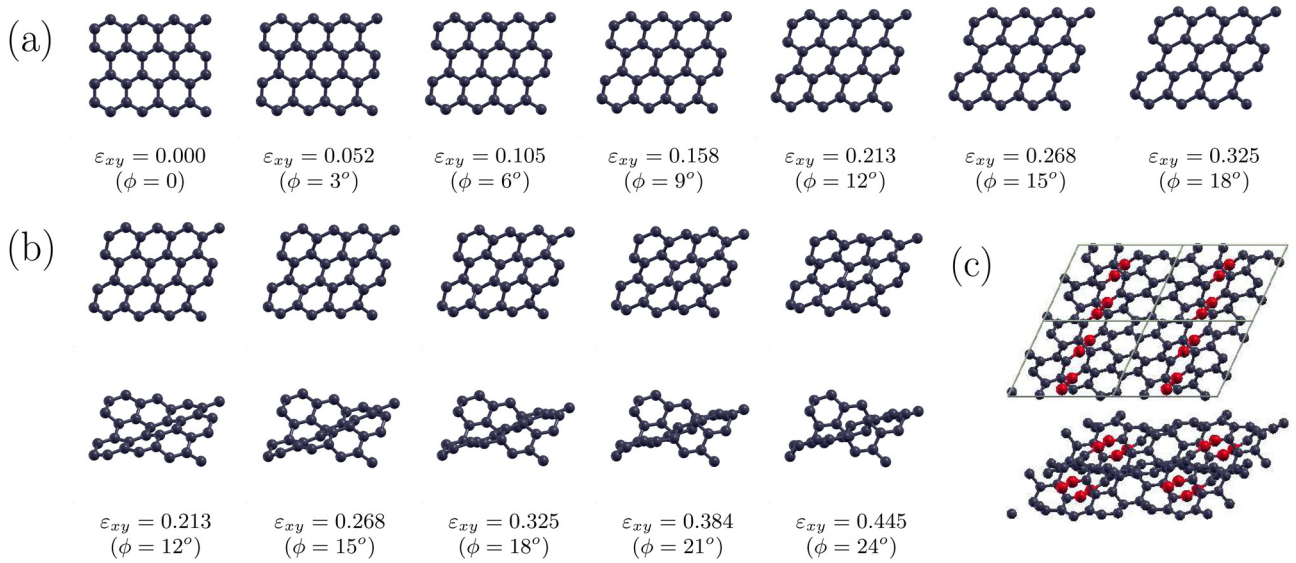

Fig. 5 Snapshots of the optimized graphene structure under in-plane shear strain, (a) when planarity is retained, (b) when buckling occurs. Top and side views are shown in (b). Below each snapshot the shear strain ε_{xy} and the tilting angle between the lattice vectors **a** and **b** are shown. (c) Top view (top panel) and side view (bottom panel) of the optimized structure obtained for graphene under in-plane shear strain ε_{xy} = 0.466, corresponding to a tilting angle ϕ = 25°. The red-colored spheres represent sp^1 atoms, while all other atoms are sp^2.

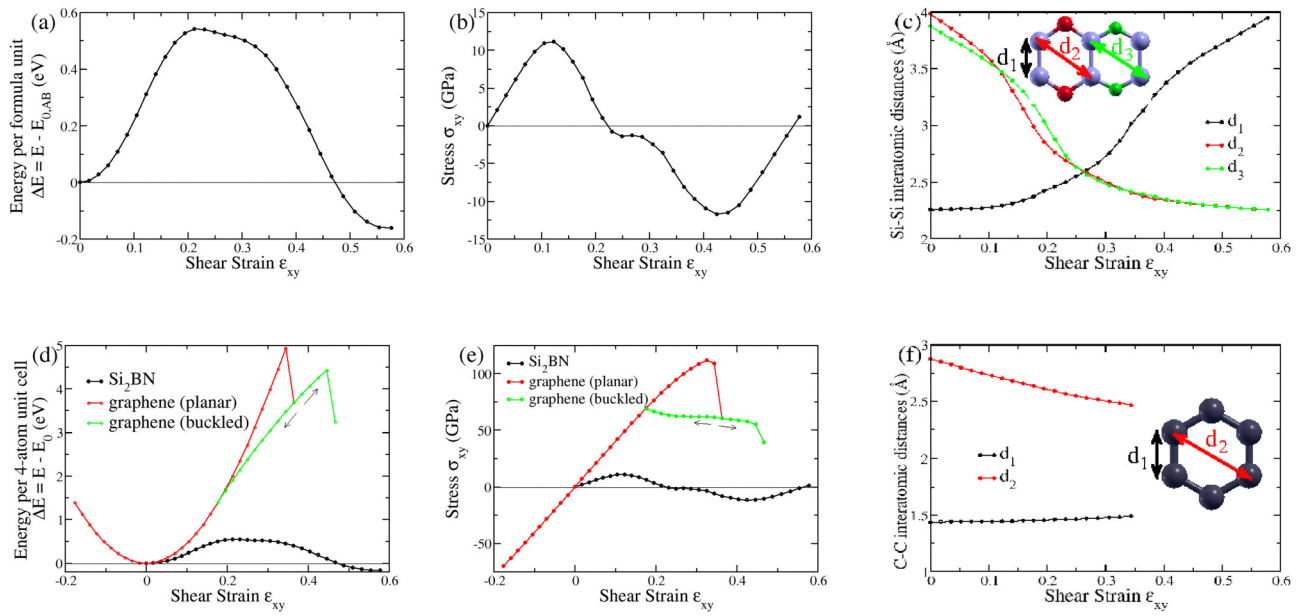

Fig. 6 (a) Strain energy per formula unit ΔE, (b) shear stress σ_{xy} and (c) Si–Si interatomic distances *versus* shear strain ε_{xy} for the conversion of AB Si_2BN into AA Si_2BN. (d) Strain energy per 4-atom unit cell ΔE, (e) shear stress σ_{xy} and (f) C–C interatomic distances *versus* shear strain ε_{xy} for graphene.

hand, the energy curve for graphene takes much higher values than those for Si_2BN. It is worth noting that the energy to break the Si–Si bonds of Si_2BN by applying uniaxial tensile strain along the direction of Si–Si bonds is of the order of 0.5 eV per atom.[8] Considering that there is one Si–Si bond per Si_2BN formula unit (four atoms), the energy to break a Si–Si bond is of the order of 2 eV.

Moreover, Fig. 6(b) and (e) show the shear stress σ_{xy} for Si_2BN and graphene, respectively, as a function of shear strain ε_{xy}. The stress–strain curve for Si_2BN is also shown in Fig. 6(e) for comparison. As one can see, for the conversion of AB Si_2BN into AA, or the opposite, the maximum shear stress that has to be applied is 11 GPa. Fitting the stress–strain curve to a cubic polynomial for ϕ in the range $-5^\circ \leq \phi \leq 5^\circ$ we found for Si_2BN, $\sigma_{xy} = 119.612\varepsilon_{xy} + 0.600703{\varepsilon_{xy}}^2 - 960.050{\varepsilon_{xy}}^3$, while for graphene, $\sigma_{xy} = 405.144\varepsilon_{xy} - 0.416954{\varepsilon_{xy}}^2 - 318.887{\varepsilon_{xy}}^3$. Using these polynomials, one can find the shear modulus G for Si_2BN and graphene, considering that for small strains $G = \sigma_{xy}/\varepsilon_{xy}$ is equal to

the coefficient of the linear term. Thus, for Si_2BN, G = 120 GPa and for graphene G = 405 GPa. This value for graphene is consistent with the one obtained using the formula $G = E/(2(1+\nu))$, which is valid for isotropic materials like graphene. In this formula, E is Young's modulus, and ν the Poisson's ratio. Considering that E and ν calculated with the same method,[8] are E = 964 GPa and ν = 0.190, one finds exactly the same value for G ($G = E/(2(1+\nu))$ = 405 GPa).

In turn, Fig. 6(c) and (d) show the evolution of the Si–Si interatomic distances d_1, d_2 and d_3 for Si_2BN, and the C–C interatomic distances d_1 and d_2 for graphene as a function of ε_{xy}. These interatomic distances are shown in the insets. As Fig. 6(c) shows, the bond length d_1 increases as a function of ε_{xy}, while d_2 and d_3 decrease. For ε_{xy} = 0.27 (or $\phi \approx 15^\circ$) the three interatomic distances become all equal and take the value $d_1 = d_2 = d_3$= 2.58 Å, corresponding to an increase of the Si–Si bond length of the order of 14%. For increasing ε_{xy} values, the new Si–Si bond is formed with bond length d_2 (or d_3), and the structure is transformed from AB into AA Si_2BN. On the other hand, Fig. 6(e) shows a totally different behavior for graphene, as already discussed above. The bond length d_1 does not change significantly *versus* ε_{xy}, while the change in the third neighbor distance d_2 is not enough to cause the breaking and the formation of new C–C bonds.

A useful practical application of the proposed phase transition would be in the field of micro-mechanical logic devices. This could be achieved by, say, assigning "0" and "1", respectively, to AA and AB stacking. A key benefit of this is that Si_2BN based systems can be used to store data by means of mechanical applications without requiring electric power. Other applications may be considered by exploiting the practically infinite shear ductility of the structure (since the structural features are retained) either in the AA or AB stacking.

In conclusion, using first-principles calculations, we report the existence of an unusual phase transition in the novel Si_2BN 2D material, transforming Si_2BN with AB stacking into Si_2BN with AA stacking and *vice versa*. This is demonstrated *via* the application of in-plane shear strain which, contrary to other 2D materials, causes no buckling at any stage of the transformation process.

Author contributions

ZGF: conceptualization, data curation, formal analysis, investigation, methodology, project administration, software, resources, supervision, validation, visualization, writing – original draft. MM: conceptualization, methodology, project administration, supervision, validation, visualization, writing – review & editing.

Data availability

All data that support the findings of this study are included in the article.

Conflicts of interest

There are no conflicts to declare.

Acknowledgements

ZGF wishes to acknowledge financial support from (i) the LESGO H2020-EIC-FETPROACT 2019–2020 project (agreement no. 952068) of the European Union and (ii) the project PRIN 2022 – Cod. 202278NHAM (PE11) CHERICH-C "Chemical and electrochemical energy storage materials from organic wastes: the treasure hidden in C-based materials" – CUP B53D23008590006, funded by the European Union – Next Generation EU in the context of the Italian National Recovery and Resilience Plan, Mission 4, Component 2, Investment 1.1, "Fondo per il Programma Nazionale di Ricerca e Progetti di Rilevante Interesse Nazionale (PRIN)".

Notes and references

1 A. N. Andriotis, E. Richter and M. Menon, *Phys. Rev. B*, 2016, **93**, 081413.
2 E. D. Sandoval, S. Hajinazar and A. N. Kolmogorov, *Phys. Rev. B*, 2016, **94**, 094105.
3 Z. G. Fthenakis, M. Jaishi, B. Narayanan, A. N. Andriotis and M. Menon, *J. Phys.: Condens. Matter.*, 2021, **33**, 165001.
4 J. P. Perdew, K. Burke and M. Ernzerhof, *Phys. Rev. Lett.*, 1996, **77**, 3865–3868.
5 J. M. Soler, E. Artacho, J. D. Gale, A. García, J. Junquera, P. Ordejón and D. Sánchez-Portal, *J. Phys.: Condens. Matter.*, 2002, **14**, 2745.
6 H. R. Mahida, D. Singh, Y. Sonvane, P. B. Thakor, R. Ahuja and S. K. Gupta, *J. App. Phys.*, 2019, **126**, 233104.
7 C.-W. Wu, C. Xiang, H. Yang, W.-X. Zhou, G. Xie, B. Ou and D. Wu, *Chin. Phys. B*, 2021, **30**, 037304.
8 Z. G. Fthenakis and M. Menon, *Phys. Rev. B*, 2019, **99**, 205302.
9 S. Hu, Y. Yong, C. Li, Z. Zhao, H. Jia and Y. Kuang, *Phys. Chem. Chem. Phys.*, 2020, **22**, 13563–13568.
10 A. M. Satawara, G. A. Shaikh, S. K. Gupta, A. N. Andriotis, M. Menon and P. Gajjar, *Int. J. Hydrogen Energy*, 2023, **48**, 25438–25449.
11 M. Jiang, J. Xu, P. Munroe, Z.-H. Xie and Z. Chen, *Int. J. Hydrogen Energy*, 2023, **50**, 865–878.
12 R. Akilan, D. Ravichandran, S. Vinnarasi and R. Shankar, *Mater. Lett.*, 2020, **279**, 128487.
13 P. Panigrahi, Y. Pal, R. Ahuja and T. Hussain, *Energy Fuels*, 2021, **35**, 12688–12699.
14 P. Panigrahi, S. B. Mishra, T. Hussain, B. R. K. Nanda and R. Ahuja, *ACS Appl. Nano Mater.*, 2020, **3**, 9055–9063.
15 V. Babar, A. Murat and U. Schwingenschlögl, *J. Phys.: Cond. Matter.*, 2020, **32**, 355602.
16 S. Thomas, A. K. Madam and M. Asle Zaeem, *Phys. Chem. Chem. Phys.*, 2022, **24**, 4394–4406.
17 D. Singh, S. Chakraborty and R. Ahuja, *ACS Appl. Energy Mater.*, 2019, **2**, 8441–8448.
18 D. S. Akilesh Muralidharan, M. Subramani and S. Ramasamy, *J. Biomol. Struct. Dyn.*, 2023, **0**, 1–32.

19 K. G. Reeves, Y. Yao and Y. Kanai, *J. Chem. Phys.*, 2016, **145**, 124705.
20 J. Zhou and S. Zhang, *npj 2D Mater. Appl.*, 2021, **5**, 16.
21 J. Zhou, S. Zhang and J. Li, *NPG Asia Mater.*, 2020, **12**, 2.
22 N. Troullier and J. L. Martins, *Phys. Rev. B: Condens. Matter Mater. Phys.*, 1991, **43**, 1993–2006.
23 L. Kleinman and D. M. Bylander, *Phys. Rev. Lett.*, 1982, **48**, 1425–1428.
24 H. J. Monkhorst and J. D. Pack, *Phys. Rev. B*, 1976, **13**, 5188–5192.
25 Z. G. Fthenakis and N. N. Lathiotakis, *Phys. Chem. Chem. Phys.*, 2015, **17**, 16418–16427.